UNIVERSITY OF GOTHENBURG

DEPARTMENT OF PHYSICS

How stable are molecular dianions?

Lifetime Calculations of C_{60}^{2-}

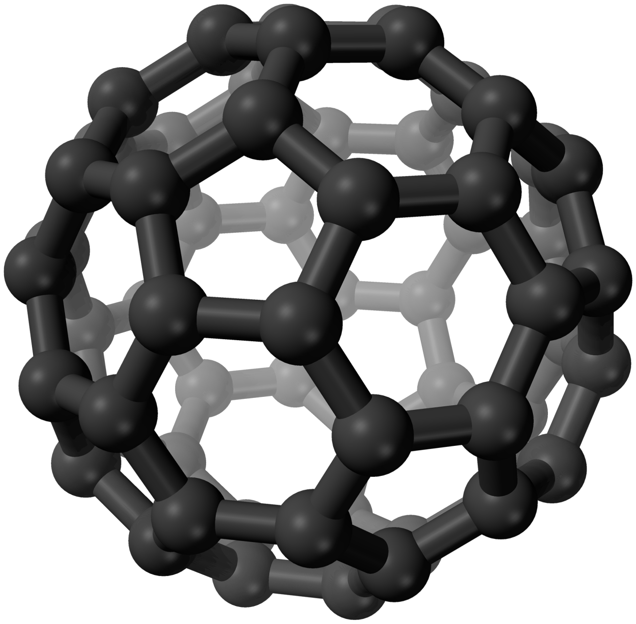

Benjamin Björnsson

Degree project for Bachelor of Science with a major in Physics
[2020], 180 HEC
First Cycle

Abstract

Since the discovery of fullerenes, the C_{60} molecule has attracted considerable attention because of its high level of symmetry and its ability to act as a platform for studying interacting electrons. It can be created as a doubly negatively charged ion in vacuum, which has raised the question of whether it is stable or meta stable. In this thesis we use a simple model to calculate the lifetime of the C_{60}^{2-} molecule. Through tunneling calculations, it is found that the lifetime should be measurable if the dianions can be stored for up to a minute.

Contents

1 Introduction 1

2 Background 3
2.1 DESIREE: The C_{60}^{2-} experiment 3
2.2 The C_{60}^{2-} model 3

3 Theoretical Background 7
3.1 Semiclassical approximation 7
3.1.1 The WKB approximation 7
3.1.2 Validity of the approximation 10
3.1.3 Connection formulae 11
3.1.4 Tunneling rate from WKB 11
3.1.5 Tunneling: The Coulomb Barrier 14
3.2 Charged particle near a charged conducting sphere 15
3.3 Electron emission 17
3.4 Heat capacity from vibrational frequencies 18
3.5 The Emission Rate 19

4 Results and Discussion 21
4.1 Tunneling rates of C_{60}^{2-} 21
4.2 Emission rate of C_{60}^{2-} for fixed ℓ 22
4.3 Emission rate of C_{60}^{2-} for different ℓ values 24

5 Conclusion 27

Chapter 1

Introduction

Before the discovery of buckminsterfullerene, or simply fullerene, there were two known allotropes of carbon; diamond and graphite. The discovery of fullerene in 1985, awarded the scientists Sir Harold W. Kroto, Richard E. Smalley and Robert F. Curl, Jr., with the Nobel prize in Chemistry in 1996.[1]

The C_{60} molecule is probably the most iconic of the fullerenes, with its high level of symmetry and the resemblance of a soccer ball. It has attracted considerable interest, since it has a number of interesting properties. For example, it can be created as a doubly negatively charged ion, or simply dianion, in vacuum.

Lifetime measurements of C_{60}^{2-} have been conducted at the ELISA storage ring at the University of Aarhus. The lifetime was measured to be in the range of 2 to 200 seconds [2]. The large uncertainty is due to that the ELISA storage ring is at room temperature. This makes it impossible to directly measure the lifetime of the molecule without support from modeling, because of excitation from black body radiation.

Low temperature experiments are therefore to be performed at the DESIREE facility at Stockholm University. The DESIREE facility is a storage ring for ions at the temperature of 10 K. Because of the low temperature, the black body radiation will not have enough energy to excite the molecules. In addition, the dianions can be stored for up to minutes, since the DESIREE storage ring is at extremely high vacuum.

In this thesis we do theoretical calculations of the emission rate of vibrationally hot C_{60}^{2-} and its inherent lifetime. These calculations are aimed for direct comparison with measurements of C_{60}^{2-} at the DESIREE facility, allowing for a detailed understanding of the cooling mechanisms.

Chapter 2

Background

In this chapter, we begin with a simple explanation of the C_{60}^{2-} experiment and we follow this discussion with an outline of the theoretical model.

2.1 DESIREE: The C_{60}^{2-} experiment

At DESIREE in Stockholm, experiments are carried out to further understand the decay dynamics of C_{60}^{2-} in the gas phase.

In figure 2.1, we show a schematics of the DESIREE storage ring that is used in the experiment. The molecules are injected at the bottom left and stored in the ring for a period of time. These molecules are created in a hot environment and therefore comes out with different temperatures, giving rise to a temperature distribution among them.

During each circulation some molecules decay by electron emission. The resulting C_{60}^{-} will not stay in the storage ring since it is deflected less by the electrostatic deflectors. The emission rate can be deduced by monitoring the number of molecules that decay. This is done by counting the molecules that decay within in the region indicated in figure 2.1, by putting a sensor where the C_{60}^{-} molecules are deflected.

2.2 The C_{60}^{2-} model

To aid in the interpretations of the experimental results, we use a simple theoretic model to estimate the lifetime and the cooling dynamics. The lifetime is calculated from the tunneling probabilities through the potential barrier that traps the second electron on the C_{60}^{2-} molecule.

We begin by thinking of C_{60}^{2-} as a single electron orbiting C_{60}^{-}. It has been argued that the potential seen by the orbiting electron is well approximated by modeling C_{60}^{-} as a charged metal sphere [3]. In figure 2.2, this potential is shown to illustrate its nature and we will derive this potential in section 3.2.

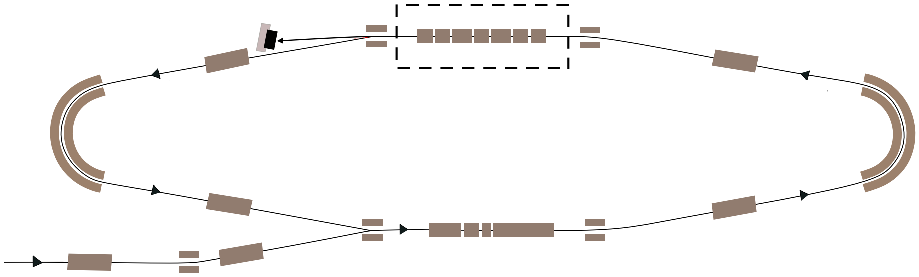

Figure 2.1: A schematic figure of the DESIREE storage ring. The molecules enter on the bottom left and circulate the storage ring. Those molecules that decay inside the dashed box are counted by the sensor.

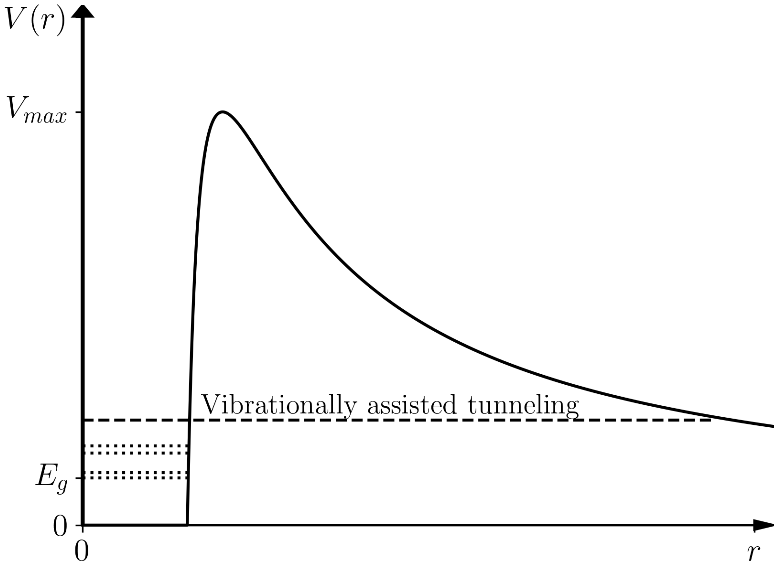

Figure 2.2: A schematics over the potential used in the model. The dotted lines are illustrations of the four energy levels. The dashed line is an illustration of the vibrational assisted tunneling.

The potential barrier has four low lying electronic states, where we use the numerical values recorded in Ref. [2]. See table 2.1. The energy levels are positioned as illustrated in figure 2.2.

The population of these energy levels depends on the internal temperature.

Table 2.1: The four energy levels assumed in the model with their corresponding degeneracy.

Energy [eV]	0.200	0.222	0.305	0.335
Degeneracy	1	5	9	9

This means that the spontaneous decay of C_{60}^{2-} will have a contribution from the four energy levels.

In addition, because of rapid decay for high internal temperature, there will be an additional decay from vibrational assisted tunneling [2]. The vibrational assisted tunneling will consist of a single energy level that acts as a decay channel for high temperature molecules. This energy level is positioned as illustrated in figure 2.2.

In the experiment, the molecules are produced internally hot where the temperature of the individual molecules are distributed according to an internal temperature distribution. The information held by the internal temperature distribution is the number of molecules of temperature T that has not yet decayed. Hence the distribution has a time dependence since when the molecules decay they are no longer in the ion beam.

In aggregate we calculate the emission rate by summing the decay over the entire ensemble. The emission rate is important since it is the quantity measured within the experiment.

Chapter 3

Theoretical Background

As described in the previous chapter, the C_{60}^{2-} emission rate is of interest since it is what is measured in the experiment. By calculating the emission rate we can get a better understanding of the decay dynamics.

In order to do so we first have to calculate the tunneling rate. We therefore derive the tunneling rate within the WKB approximation. When calculating the tunneling rates within this approximation, we need an expression for the potential barrier. We therefore derive the potential assumed by the model.

We also described in section 2.2 that the molecules are created in a hot environment. The molecules are vibrationally hot, which led to the notion of an internal temperature distribution where each of the molecule has its own internal temperature. The internal temperature distribution will depend on the vibrational heat capacity of C_{60}. We therefore calculate the vibrational heat capacity using calculated vibrational frequencies.

3.1 Semiclassical approximation

We derive the WKB approximation, which finds approximate solutions to the time independent Schrödinger equation in slowly varying potentials. Motivated by classical physics, we introduce a local momentum accompanied with a local de Broglie wavelength. We find approximate wave functions in the regions far from the classical turning points. Using these approximate solutions together with the so called connection formulae we find the WKB tunneling rate of a particle through a barrier. The derivations of this section are based on the lecture notes written by Barton Zwiebach [4].

3.1.1 The WKB approximation

Motivated by classical mechanics we think of a particle of mass m with energy E, moving in a potential $V(\vec{x})$. This particle can be thought of as having a local momentum $p(\vec{x})$, given by

$$p^2(\vec{x}) = 2m(E - V(\vec{x})). \tag{3.1}$$

For future reference, we introduce the functions $k^2(\vec{x}) > 0$ and $\kappa^2(\vec{x}) > 0$, given by

$$\hbar^2 k^2(\vec{x}) = 2m(E - V(\vec{x})) = p^2(\vec{x}) \quad \text{when} \quad E > V(\vec{x}), \tag{3.2}$$

$$\hbar^2 \kappa^2(\vec{x}) = 2m(V(\vec{x}) - E) = -p^2(\vec{x}) \quad \text{when} \quad E < V(\vec{x}), \tag{3.3}$$

where $E > V(\vec{x})$ and $E < V(\vec{x})$ denote the classically allowed and classically forbidden regions, respectively. Using the local momentum in (3.1) we can define a local de Broglie wavelength as

$$\lambda(\vec{x}) = \frac{h}{p(\vec{x})} = \frac{2\pi\hbar}{p(\vec{x})}. \tag{3.4}$$

We know that quantum effects become less relevant as the de Broglie wavelength becomes small, compared to the relevant size of the system (think of the slit experiment as the slit becomes large). We can think of $\hbar$ as a small, variable parameter, as if having a set of parallel universes with different values of $\hbar$. In these parallel universes, quantum mechanical effects becomes relevant for different length scales of our system. Note from (3.4) that $\lambda \to 0$ as $\hbar \to 0$, and quantum effects are gradually removed. We can hence expand our wave function in a power series of $\hbar$, thinking of $\hbar$ as a small parameter. We discuss the validity of this approximation in section 3.1.2.

So far we have introduced some notation as well as the concept of the local de Broglie wavelength. In order to connect with quantum mechanics, we recall the time-independent Schrödinger equation

$$-\frac{\hbar^2}{2m}\nabla^2\psi(\vec{x}) = (E - V(\vec{x}))\psi(\vec{x}). \tag{3.5}$$

We can write this, using the local momentum, as

$$\hat{\mathbf{p}}^2\nabla^2\psi(\vec{x}) = p^2(\vec{x})\psi(\vec{x}), \tag{3.6}$$

where $\hat{\mathbf{p}}$ is the quantum mechanical momentum operator. Without any loss of generality, we write the complex valued wave function as

$$\psi(\vec{x}) = \sqrt{\rho(\vec{x})}e^{\frac{i}{\hbar}S(\vec{x})}, \tag{3.7}$$

where $S(\vec{x})$ is a real function and $\rho(\vec{x})$ is the probability density function. Absorbing $\sqrt{\rho(\vec{x})}$ into $S(\vec{x})$, we have that

$$\psi(\vec{x}) = e^{\frac{i}{\hbar}S(\vec{x})}, \tag{3.8}$$

where $S(\vec{x})$ is now a complex valued function. Substituting this into (3.6), we have that

$$-\hbar^2\left(\frac{i}{\hbar}\nabla^2 S(\vec{x})) - \frac{1}{\hbar^2}(\nabla S(\vec{x}))^2\right)e^{\frac{i}{\hbar}S(\vec{x})} = p^2(\vec{x})e^{\frac{i}{\hbar}S(\vec{x})}, \tag{3.9}$$

and by canceling the exponentials, we are left with

$$(\nabla S(\vec{x}))^2 - i\hbar\nabla^2 S(\vec{x}) = p^2(\vec{x}). \tag{3.10}$$

At this point, we have rewritten the Schrödinger equation in an unusual form, without changing the physics. The change in physics comes from expanding the $S(\vec{x})$ in a power series of $\hbar$, where we think of $\hbar$ as a small parameter. We write

$$S(\vec{x}) = S_0(\vec{x}) + \hbar S_1(\vec{x}) + O(\hbar^2), \tag{3.11}$$

where $S_0(\vec{x})$ has units of $\hbar$ and $S_1(\vec{x})$ has no units. Substituting into (3.10), we have that

$$\left(\nabla S_0(\vec{x}) + \hbar\nabla S_1(\vec{x}) + O(\hbar^2)\right)^2 - i\hbar\left(\nabla^2 S_0(\vec{x}) + O(\hbar)\right) = p^2(\vec{x}), \tag{3.12}$$

and by rearranging in powers of $\hbar$, we are left with

$$\left((\nabla S_0(\vec{x}))^2 - p^2(\vec{x})\right) + \hbar\left(2\nabla S_0(\vec{x})\nabla S_1(\vec{x}) - i\nabla^2 S_0(\vec{x})\right) + O(\hbar^2) = 0. \tag{3.13}$$

For this equation to be identically zero for all values of $\hbar$, each coefficient must be identically zero. Continuing with the one dimensional equation, we have for the first two coefficients that

$$S_0'(x) = \pm p(x), \tag{3.14}$$

$$S_1'(x) = \frac{i}{2}\frac{S_0''(x)}{S_0'(x)} = \frac{i}{2}\frac{p'(x)}{p(x)} = \frac{i}{2}\frac{d}{dx}\ln(p(x)), \tag{3.15}$$

where primes denote derivatives with respect to the argument. By integrating from x_0 to x, we have that

$$S_0(x) = \pm\int_{x_0}^{x} p(x')dx', \tag{3.16}$$

$$S_1(x) = \frac{i}{2}\ln(p(x)) + C, \tag{3.17}$$

where C is a constant of integration. Combining these expressions with (3.11) and (3.8), and by ignoring orders of $\hbar^2$, we have that the approximate wave function can be written as

$$\psi(x) = \exp\left(\frac{i}{\hbar}\left(\pm\int_{x_0}^{x} p(x')dx' + \hbar\frac{i}{2}\ln(p(x)) + C\right)\right), \tag{3.18}$$

$$= \frac{A}{\sqrt{p(x)}}\exp\left(\pm\frac{i}{\hbar}\int_{x_0}^{x} p(x')dx'\right). \tag{3.19}$$

Using this result with (3.2) and (3.3), we have the two general solutions

$$\psi(x) = \frac{A}{\sqrt{k(x)}}\exp\left(i\int_{x_0}^{x} k(x')dx'\right) + \frac{B}{\sqrt{k(x)}}\exp\left(-i\int_{x_0}^{x} k(x')dx'\right), \tag{3.20}$$

$$\psi(x) = \frac{C}{\sqrt{\kappa(x)}}\exp\left(\int_{x_0}^{x} \kappa(x')dx'\right) + \frac{D}{\sqrt{\kappa(x)}}\exp\left(-\int_{x_0}^{x} \kappa(x')dx'\right), \tag{3.21}$$

$$\tag{3.22}$$

in the classically allowed and classically forbidden regions, respectively. Note how the solution in the classically allowed region looks like an ordinary plane waves, whereas the solution in the classically forbidden region looks like growing and decaying exponentials. In order to solve a particular problem, we are faced with the problem of connecting the coefficients A, B, C, and D. Since the local de Broglie wavelength becomes infinite near the turning points, the connection cannot be achieved by usual boundary approach. This connection is instead accomplished through the so called connection formulae, which is described in section 3.1.3.

When we have found our solutions, we are often interested in the probability current in different regions of space. We begin by recalling the usual form of the probability current, namely

$$\mathbf{J} = \frac{\hbar}{m}\mathrm{Im}\left(\psi^*(x)\frac{d\psi(x)}{dx}\right). \tag{3.23}$$

Later in this chapter, we will be particularly interested in the probability current of right going waves in the classically allowed regions. Hence from (3.20), we have that

$$\frac{d\psi(x)}{dx} = \frac{A}{\sqrt{k(x)}}\left(-\frac{k'(x)}{2k(x)} + ik(x)\right)\exp\left(i\int_{x_0}^{x} k(x')dx'\right), \tag{3.24}$$

or by substitution in (3.23), we have that

$$\mathbf{J} = \frac{\hbar|A|^2}{m}. \tag{3.25}$$

3.1.2 Validity of the approximation

We noted in the the previous section that the local de Broglie wavelength becomes infinite at the turning points. Hence for the approximate solution to be valid, we will have to restrict ourselves to regions of space far enough from the turning points. Furthermore, we can argue from looking at (3.13), that the second order term must be much smaller than the first order term. We can express this by writing

$$\hbar|S_0'(x)S_1'(x)| \ll |S_0'(x)|^2 \tag{3.26}$$

or by recalling (3.14) and (3.15), we have that

$$\hbar\left|\frac{p'(x)}{p(x)}\right| \ll p(x). \tag{3.27}$$

By using (3.4), we have that

$$\hbar\left|\frac{p'(x)}{p^2(x)}\right| = \left|\frac{d}{dx}\frac{\hbar}{p(x)}\right| = \left|\frac{d\lambda(x)}{dx}\right| \ll 1. \tag{3.28}$$

Multiplying both sides by $\lambda(x)$ we arrive at the final expression

$$\lambda(x)\left|\frac{d\lambda(x)}{dx}\right| \ll \lambda(x). \tag{3.29}$$

We also have from (3.1) that $|p(x)p'(x)| = mV'(x)$, which can be used in (3.27), giving us

$$\frac{1}{m}\frac{\hbar}{p(x)}\left|\frac{p'(x)}{p^2(x)}\right| \simeq \lambda(x)\left|\frac{dV(x)}{dx}\right| \ll \frac{p^2(x)}{2m}. \tag{3.30}$$

We see from (3.28) that the approximation is valid as long as the local de Broglie wavelength is slowly varying. Similarly from (3.29), we see that the local de Broglie wavelength should not change significantly over a length of the local de Broglie wavelength. In terms of the potential in (3.30), we see that the potential energy should not change significantly in comparison to the kinetic energy over a length of the local de Broglie wavelength.

3.1.3 Connection formulae

As mentioned in section 3.1.1, in order to find a solution to a given problem, we have to connect the coefficients in (3.22) and (3.20). This is done by the connection formulae that are asymptotic solutions to the Airy differential equation. We will not derive the connection formulae but merely state the result that is needed in the next section. However, a derivation of the result can be found in the reference [4].

We will need the connection formulas that connect through a potential barrier from right to left given by

$$\frac{2}{\sqrt{k(x)}}\cos\left(\int_x^a k(x')dx' - \frac{\pi}{4}\right) \Longleftarrow \frac{1}{\sqrt{\kappa(x)}}\exp\left(-\int_a^x \kappa(x')dx'\right), \tag{3.31}$$

$$\frac{1}{\sqrt{k(x)}}\sin\left(\int_b^x k(x')dx' - \frac{\pi}{4}\right) \Longrightarrow -\frac{1}{\sqrt{\kappa(x)}}\exp\left(\int_x^b \kappa(x')dx'\right). \tag{3.32}$$

The first equation says that if we have a decaying exponential, as we move to the right, inside the barrier it can be connected to an oscillatory solution to the left of the turning point with the cosine behavior. The second equation says that if we have a sinus behavior to the right of the turning point we can connect it to a growing exponential, as we move to the right, inside the barrirer.

3.1.4 Tunneling rate from WKB

We know from classical mechanics that for a particle with energy E, trapped in a potential $V(x)$, the particle oscillates between the two classical turning points a and b. See figure 3.1. However, from quantum mechanics, we know that for a localized wave function inside the barrier, there will be a leakage over time, resulting in a wave function to the right of c. We denote the incident and reflected wave functions at b as $\psi_i(x)$ and $\psi_r(x)$, respectively. In addition, we denote the wave function inside the barrier $\psi_b(x)$ and the transmitted wave to the right of the barrier $\psi_t(x)$.

Since the wave function $\psi_t(x)$ for $x \gg c$ is a wave traveling to the right, we have from (3.20) that

$$\psi_t(x) = \frac{F}{\sqrt{k(x)}} \exp\left(i \int_c^x k(x')dx' - i\frac{\pi}{4} \right), \tag{3.33}$$

where we have added a constant phase for convenience. By expanding the complex exponential, we can write this as

$$\psi_t(x) = \frac{F}{\sqrt{k(x)}} \left[\cos\left(i \int_c^x k(x')dx' - i\frac{\pi}{4} \right) + i \sin\left(i \int_c^x k(x')dx' - i\frac{\pi}{4} \right) \right]. \tag{3.34}$$

Using the connection formula (3.32), we can connect the sin-term to the wave function $\psi_b(x)$ (an exponential growing as we move to the left), giving us

$$\psi_b(x) = -\frac{iF}{\sqrt{\kappa(x)}} \exp\left(\int_x^c \kappa(x')dx' \right), \quad b \ll x \ll c. \tag{3.35}$$

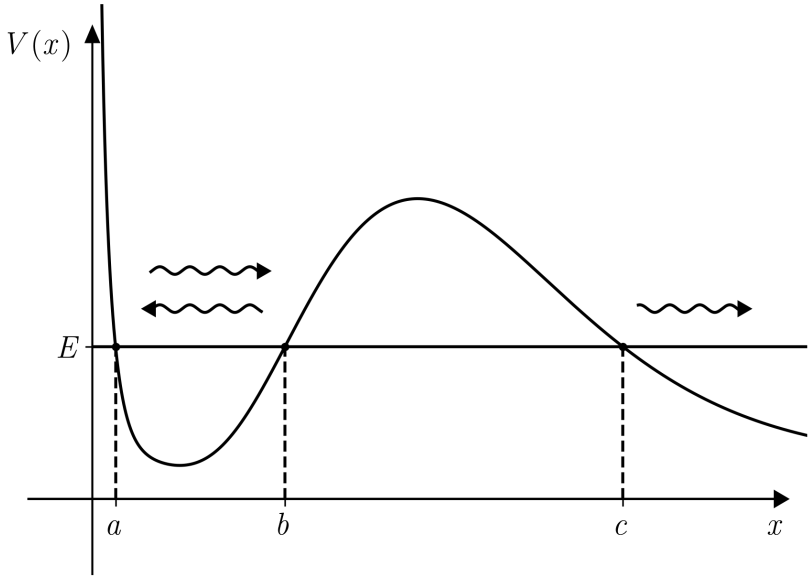

Figure 3.1: An illustration of a wave function localized in a potential barrier with a wave leaking through the barrier.

We can rewrite this as

$$\psi_b(x) = -\frac{iF}{\sqrt{\kappa(x)}} \exp\left(\int_b^c \kappa(x)dx - \int_b^x \kappa(x')dx'\right), \tag{3.36}$$

by separating the integral. We define

$$\theta = \int_b^c \kappa(x)dx, \tag{3.37}$$

and note that (3.36) can be written as

$$\psi_b(x) = -\frac{iFe^{\theta}}{\sqrt{\kappa(x)}} \exp\left(-\int_b^x \kappa(x')dx'\right) \quad b \ll x \ll c. \tag{3.38}$$

Now looking from inside the barrier, $\psi_b(x)$ is a decaying exponential as we are move to the right. This can be connected to the wave function $\psi(x)$ on the left of b by the connection formula (3.31), giving us

$$\psi(x) = -\frac{i2Fe^{\theta}}{\sqrt{k(x)}} \cos\left(\int_x^b k(x')dx' - \frac{\pi}{4}\right) \tag{3.39}$$

$$= -\frac{iFe^{\theta}}{\sqrt{k(x)}} \left[\exp\left(i\int_x^b k(x')dx' - i\frac{\pi}{4}\right) + \exp\left(-i\int_x^b k(x')dx' - i\frac{\pi}{4}\right)\right]. \tag{3.40}$$

We recognize that the wave function $\psi(x)$ inside the barrier is now in the form of $\psi(x) = \psi_i(x) + \psi_r(x)$, giving us that

$$\psi_i(x) = -\frac{iFe^{\theta}}{\sqrt{k(x)}} \exp\left(-i\int_x^b k(x')dx' + i\frac{\pi}{4}\right). \tag{3.41}$$

We are now in the position of calculating the transmission coefficient by taking the ratio of currents from the transmitted and incident wave functions, $\mathbf{J}_t$ and $\mathbf{J}_i$, respectively. Comparing (3.33) and (3.41) to (3.20), and by using (3.25), we have that

$$T = \frac{\mathbf{J}_t}{\mathbf{J}_i} = \frac{|F|^2}{|-iFe^{\theta}|^2} = e^{-2\theta}, \tag{3.42}$$

or by recalling (3.37), we have the well known result

$$T = \exp\left(-2\int_b^c \kappa(x)dx\right), \tag{3.43}$$

for the WKB transmission coefficient. We can think of this transmission coefficient as the probability that the particle transitions each time the particle reaches the turning point b. The time it takes for a classical particle to go from b to a and back to b is given by

$$\Delta t = 2\int_a^b \frac{dx}{v(x)} = 2m\int_a^b \frac{dx}{p(x)}. \tag{3.44}$$

The reciprocal of this is the number of time per unit time the particle reaches b. Multiplying by T, we have the WKB tunneling rate, given by the relation

$$\frac{1}{R} = \frac{\Delta t}{T} = 2m\int_a^b \frac{dx}{p(x)} \exp\left(2\int_a^b \kappa(x)dx\right). \tag{3.45}$$

3.1.5 Tunneling: The Coulomb Barrier

We can use (3.45) to find a closed form formula for the tunneling rate of the Coulomb barrier, illustrated in figure 3.2. We do this since the potential we are interested in have no such form. Hence the Coulomb barrier is used as a sanity check for our numerical calculations.

The Coulomb barrier is given by

$$V(r) = \begin{cases} V_0, & 0 < r < r_1, \\ \frac{k_e}{r}, & r \geq r_1, \end{cases} \tag{3.46}$$

in SI units. Since the potential is constant on the left of the barrier the time Δt is given by

$$\Delta t = 2m\int_0^b \frac{dr}{\sqrt{2m(E-V_0)}} = b\sqrt{\frac{2m}{(E-V_0)}}. \tag{3.47}$$

We use (3.37) inside the barrier where $E = \frac{k_e}{c}$, giving us

$$\theta = \sqrt{\frac{2m}{\hbar^2}}\int_b^c dr\sqrt{\frac{k_e}{r} - E}, \tag{3.48}$$

$$= \sqrt{\frac{2mE}{\hbar^2}}\int_b^c dr\sqrt{\frac{c}{r} - 1}, \tag{3.49}$$

$$= \sqrt{\frac{2mE}{\hbar^2}}\left[c\cos^{-1}\left(\frac{b}{c}\right) - \sqrt{b(c-b)}\right]. \tag{3.50}$$

Substituting (3.47) and (3.50) in (3.45) we have the tunneling rate

$$\frac{1}{R} = b\sqrt{\frac{2m}{(E-V_0)}} \exp\left(\sqrt{\frac{2mE}{\hbar^2}}\left[c\cos^{-1}\left(\frac{b}{c}\right) - \sqrt{b(c-b)}\right]\right). \tag{3.51}$$

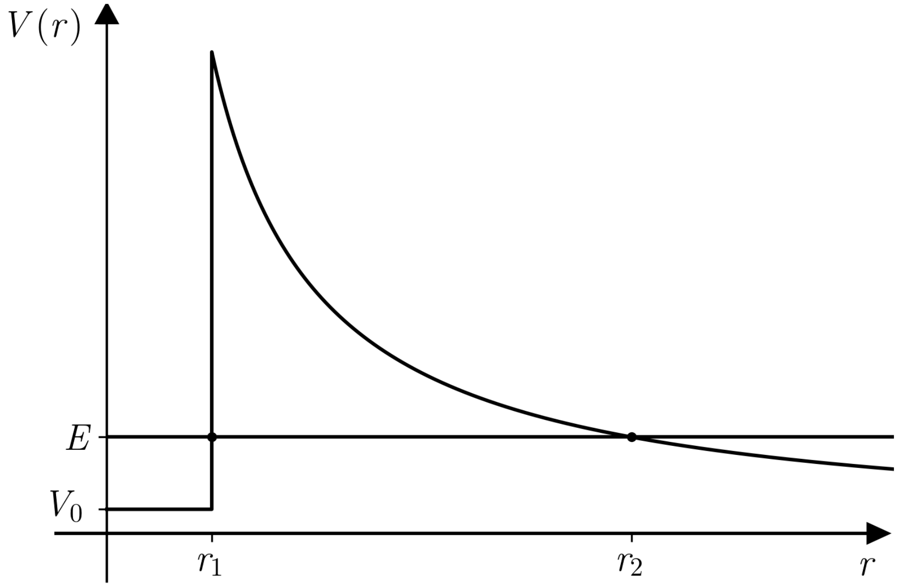

Figure 3.2: The Coulomb barrier with a localized particle with energy E.

3.2 Charged particle near a charged conducting sphere

As described in section 2.2, we model the molecule as an electron that is circulating a charged conducting sphere. We now want to derive the potential of such a system.

To derive this potential, we start with the situation illustrated in figure 3.3. We have a charge q at a distance x from the center of a conducting sphere. When the charge approaches the sphere, there will be an induced charge on the surface of the sphere, so as to keep the potential constant on the surface of the sphere. This can be achieved by putting an imaginary image charge q_i at a distance D from the center of the sphere. The potential at r is then given by

$$\Phi(\vec{r}) = \frac{k_e q_i}{r_1} + \frac{k_e q}{r_2}, \tag{3.52}$$

where k_e the electrostatic constant. By setting the potential to zero, we have that

$$\frac{r_2}{r_1} = -\frac{q}{q_i}, \tag{3.53}$$

which says that the ratio of distances are constant on the equipotential. This is the equation of a circle if the charges are of different signs. Using this for the

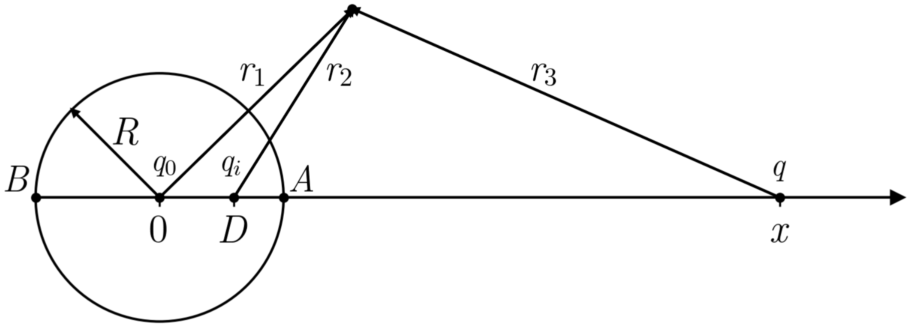

Figure 3.3: Schematics of the situation with a particle of charge q at a distance x from a charged conducting sphere.

points A and B, we force the potential to be zero at the surface of the sphere. This gives us that

$$\frac{x-R}{R-D} = \frac{x+R}{R+D}, \tag{3.54}$$

or by solving for D, we have that

$$D = \frac{R^2}{x}. \tag{3.55}$$

We also have from applying (3.53) to the point A that

$$q_i = -q\frac{r_1}{r_2} = -q\frac{R-D}{x-R}, \tag{3.56}$$

or by using (3.55), we have that

$$q_i = -q\frac{R-\frac{R^2}{x}}{x-R} = -\frac{qR}{x}. \tag{3.57}$$

In order to adjust the potential on the surface of the sphere, we introduce another imaginary charge q_0 at the center of the sphere, given by

$$q_0 = q - q_i, \tag{3.58}$$

where we have defined q_0 in such a way that the total charge of the sphere equals q. We now have that the electric field can be written as

$$E(x) = \frac{k_e q_0}{x^2} + \frac{k_e q_i}{(x-D)^2}, \tag{3.59}$$

along the x-axis, where we have left out the electric field of the charge q at x. By substituting (3.55), (3.57) and (3.58), we have that

$$E(x) = \frac{k_e q}{x^2} + \frac{k_e qR}{x^3} - \frac{k_e qRx}{(x^2-R^2)^2}. \tag{3.60}$$

We can integrate the electric field in order to find the potential at x, giving us that

$$\begin{aligned} V(x) &= -\int_{\infty}^{x} E(x')dx' && (3.61)\\ &= -\int_{\infty}^{x} \left(\frac{k_e q}{x'^2} + \frac{k_e qR}{x'^3} - \frac{k_e qRx'}{(x'^2 - R^2)^2}\right) dx' && (3.62)\\ &= \frac{k_e q}{x} + \frac{k_e qR}{2x^2} - \frac{k_e qR}{2(x^2 - R^2)}, && (3.63) \end{aligned}$$

or by rearranging we have

$$V(x) = \frac{k_e q}{x} - \frac{k_e qR^3}{2x^2(x^2 - R^2)^2}. \tag{3.64}$$

In order to get the effective potential $V_{\text{eff}}(x)$, we add the centrifugal barrier, giving us

$$V_{\text{eff}}(x) = \frac{k_e q}{x} - \frac{k_e qR^3}{2x^2(x^2 - R^2)^2} + \frac{\hbar^2 \ell(\ell + 1)}{2mx^2}. \tag{3.65}$$

This potential is illustrated in figure 3.4 for $\ell = 0, 1, 2, 3$ along with the dotted Coulomb barrier for comparison.

3.3 Electron emission

If the C_{60}^{2-} molecule had had only one electron state, we would have found the rate constant directly from (3.45). However, since we have multiple electron states, we take into account the probability distribution as a function of temperature. If we for now ignore the contribution from the vibrational assisted tunneling, the total rate is then given by the expectation value.

We begin by recalling the Boltzmann distribution. We have that for a state with energy E_i, the probability is given by

$$p_i(T) = \frac{g_i}{Z} e^{-\frac{E_i}{k_B T}}, \tag{3.66}$$

where g_i is the degeneracy and Z is the partition function given by

$$Z = \sum_i g_i e^{-\frac{E_i}{k_B T}}. \tag{3.67}$$

In order to arrive at the total rate constant, we use (3.45) to calculate a rate R_i for each energy level. Combining the tunneling rate R_i with the probability $p_i(T)$, we have that the total rate $k(T)$ is given by

$$\begin{aligned} k(T) = E[R] &= \sum_i R_i p_i \\ &= \sum_i \frac{R_i g_i}{Z} e^{-\frac{E_i}{k_B T}}. \end{aligned} \tag{3.68}$$

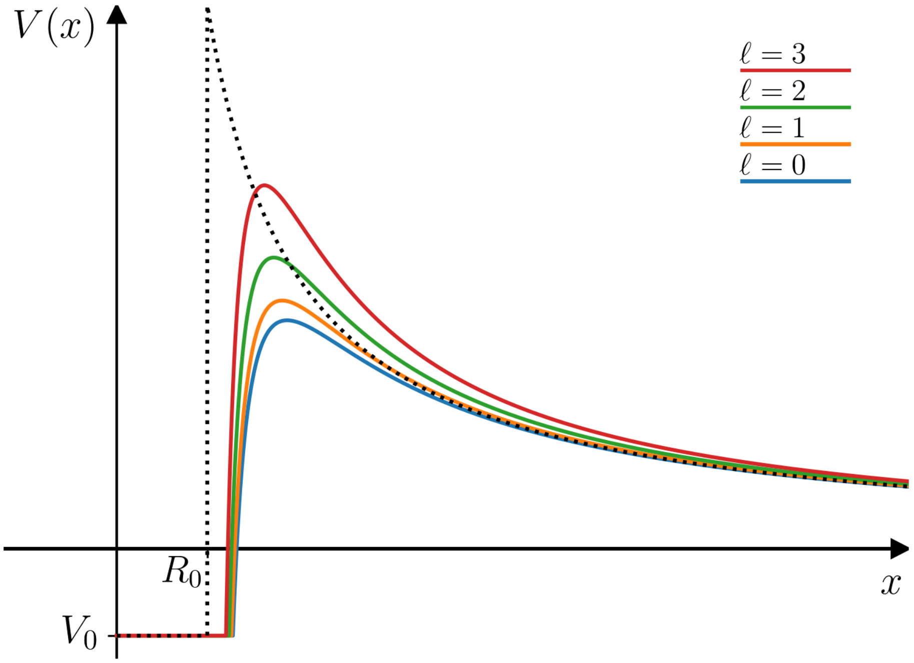

Figure 3.4: The effective potential in (3.65) for $\ell < 4$. The dotted line is the Coulomb barrier in (3.46).

3.4 Heat capacity from vibrational frequencies

In the next section when we introduce the internal temperature distribution, it will depend on the vibrational heat capacity of the C_{60} molecule.

Therefore we now derive the vibrational heat capacity of the C_{60} molecule. We begin by considering the vibrational modes of the molecule. The molecule consists of $N = 60$ carbon molecules, each having three degrees of freedom. Subtracting the three translational and the three rotational degrees of freedom we are left with $3N - 6 = 174$ modes of vibration. These vibrational frequencies can be calculated and are tabulated in various places. Using Bose-Einstein statistics, we can then evaluate the heat capacity $C_v(T)$ associated with these vibrational frequencies.

In Bose-Einstein statistics the expected number of particles in a state of energy ϵ_i and degeneracy g_i is given by

$$\langle N \rangle_i = \frac{g_i}{e^{\beta \epsilon_i} - 1}, \tag{3.69}$$

where $\beta^{-1} = k_B T$ is given by the Boltzmann's constant k_B and the absolute temperature T. Multiplying by the energy ϵ_i and summing over i, we have the expected energy given by

$$\langle E\rangle = \sum_i \frac{g_i\epsilon_i}{e^{\beta\epsilon_i}-1}. \tag{3.70}$$

In order to reach the heat capacity we simply take the derivative with respect to the temperature, giving us

$$C_v(T) = \frac{\partial\langle E\rangle}{\partial T} = \frac{\partial\langle E\rangle}{\partial\beta}\frac{\partial\beta}{\partial T} \tag{3.71}$$

$$= \frac{1}{k_BT^2}\sum_i \frac{g_i\epsilon_i^2}{(e^{\beta\epsilon_i}-1)^2}. \tag{3.72}$$

Using tabulated frequencies, we have plotted the heat capacity in figure 3.5 where the dashed line is a linear fit from reference [5].

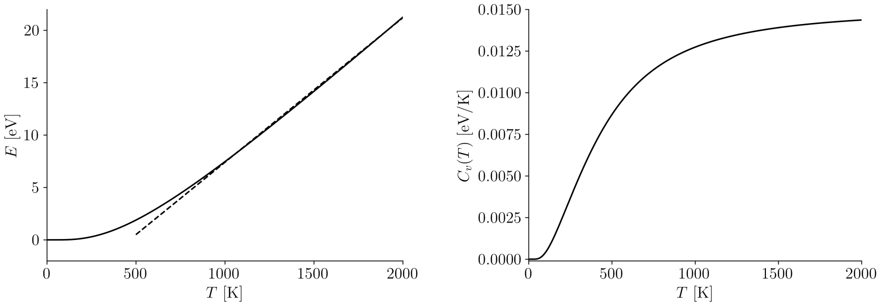

(a)

(b)

Figure 3.5: (a) Shows the expected energy where the dashed line is a linear fit in the range 1000-2000 K. (b) Shows the heat capacity.

3.5 The Emission Rate

Here we derive the emission rate by combining the results derived in this chapter. To do so we first have to define the effective rate constant $k_{\text{eff}}(T)$.

The effective rate constant will consist of two terms. The first term is $k_1(T)$ and it comes from the tunneling rates of the four energy levels, as derived in section 3.3. The second term is $k_0(T)$ and it comes from the vibrational assisted tunneling, which is added to account for the high temperature decay. The vibrational assisted tunneling is calculated in a similar way as for the four energy levels, by assuming an energy level that acts as a decay channel for high temperature molecules.

As described in section 2.2, we assume a temperature distribution over the molecules. This temperature distribution describes the number of molecules of temperature T that has not yet decayed. We use the distribution given by [2][6]

$$\begin{aligned} g(T, T_{\mathrm{i}}, t) = & \exp\left(-\alpha(T - T_{\mathrm{i}})\right) \\ & \times \left[1 + \mathrm{erf}\left(\frac{T - T_{\mathrm{i}} - f^2\alpha\sigma^2}{\sqrt{2}f\sigma}\right)\right] e^{-k_{\mathrm{eff}}(T)t}, \end{aligned} \tag{3.73}$$

where $\alpha = 1\ \mathrm{eV}(C_v(T))^{-1}$, $\sigma = \alpha\sqrt{k_B C_v(T_{\mathrm{i}})}T_{\mathrm{i}}$, T_{i} is the initial temperature when the molecules are created, f is a function of T_{i} and $C_v(T)$ is the heat capacity in (3.72) in units of eV.

By multiplying the temperature distribution with the effective rate constant, we get the contribution to the emission rate as a function of temperature. To account for the molecules of the entire cluster, we sum over the temperature giving us the final expression [6]

$$I(t) = \int dT k_{\mathrm{eff}}(T) g(T, T_{\mathrm{i}}, t). \tag{3.74}$$

Chapter 4

Results and Discussion

In the previous chapter, we derived the theoretical expressions that are needed to model the decay of C_{60}^{2-} and we now use these results to look at predictions of this theory.

4.1 Tunneling rates of C_{60}^{2-}

We first want to calculate the tunneling rates for the ground state and the three electronically excited states. To do so we first specify the parameters of the potential in (3.65). It has been suggested that $\ell < 3$ [7][8], and that $R = 4.55$ Å [3] and we plot the potential using these values in figure 4.1. In table 4.1, we tabulate the tunneling rates for the four energy levels and the three different potential forms, which has been calculated using (3.45).

Table 4.1: Calculated tunneling rates in units of s^{-1} for the four energy levels and $\ell < 3$.

	$E = 0.200$ eV	0.222 eV	0.305 eV	0.335 eV
$\ell = 0$	1.52	2.20×10	3.34×10^4	2.34×10^5
1	6.06×10^{-1}	8.79	1.35×10^4	9.54×10^4
2	1.01×10^{-1}	1.47	2.34×10^3	1.67×10^4

The decay rate for the first excited state is roughly one order of magnitude larger than that of the ground state. Furthermore, the decay rate for the second and third excited states are roughly four and five orders of magnitude larger than that of the ground state, respectively. We also see that the decay rate depends on the ℓ value, where larger ℓ gives lower decay rate. This is expected since the potential barrier is higher for higher ℓ value.

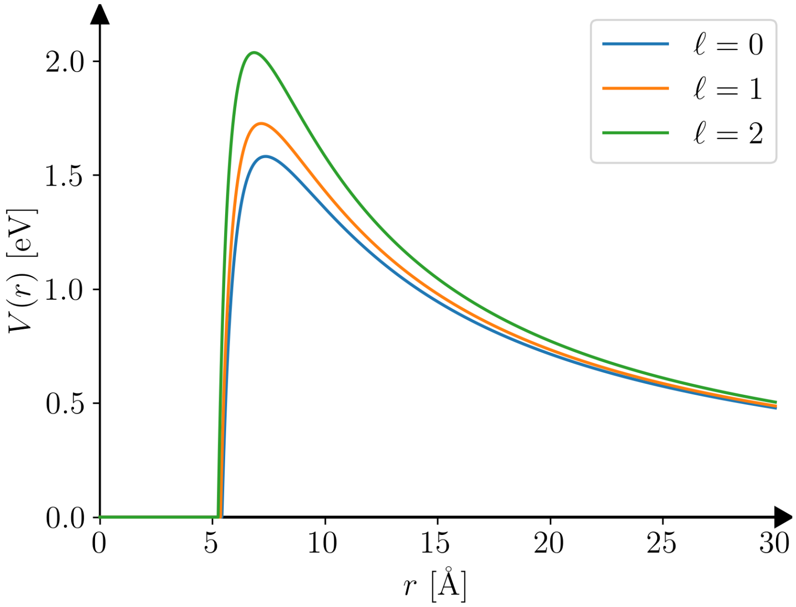

Figure 4.1: The potential in (3.65) for $R = 4.55$ Å and $\ell < 3$.

4.2 Emission rate of C_{60}^{2-} for fixed ℓ

To understand the emission rate, we begin by looking at the potential with $\ell = 1$ as was also done in reference [2]. For this reason, we begin by looking at the two contributions to the effective rate constant as described in section 3.5.

The contribution from the vibrational assisted tunneling can be understood by plotting the product of the room temperature Boltzmann $e^{-\beta E}$ and the tunneling rate in (3.45). See figure 4.2b. We approximate the peak by a single energy level, since the overwhelming contributing to the high temperature decay comes from the energies around $E = 0.452$ eV. To model this process, we follow reference [2] and assume an Arrhenius type decay, which is calculated using

$$k_0(T) = R_v e^{-\beta E_a}, \tag{4.1}$$

where R_v is the tunneling rate of the energy level of the vibrational assisted tunneling, and E_a is the activation energy given by the energy level relative to the ground state. We have that $E_a = 0.452 - 0.200 = 0.252$ eV and using (3.45) we have that $R_v = 2.73 \times 10^7\ s^{-1}$.

The contribution from the energy levels are calculated using (3.68) and the decay rates for $\ell = 1$ in table 4.1. In figure 4.3a, we plot the effective rate constant and its two contributions. To better understand where each rate is dominant we have plotted the contributions relative to $k_{\text{eff}}(T)$ in figure 4.3b. We clearly see that the vibrational assisted tunneling is dominant for high internal temperature whereas the four energy levels are dominant for low internal temperatures.

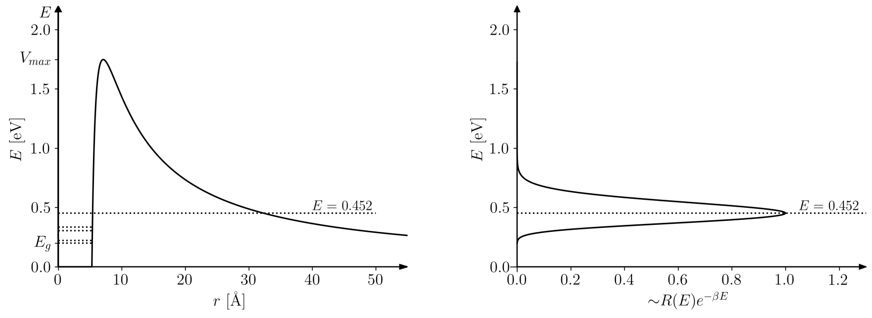

(a) (b)

Figure 4.2: (a) The potential with $\ell = 1$ and $R = 4.55$ Å. The dotted lines are the four energy levels, and the dashed line is the vibrational assisted tunneling. (b) The product of the room temperature Boltzmann $e^{-\beta E}$ and the tunneling rate.

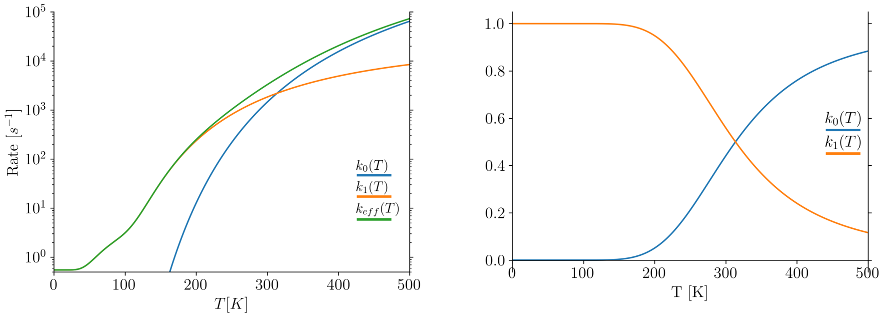

(a) (b)

Figure 4.3: (a) The effective rate constant as well as its two contributing factors. (b) Shows the two contributing factors relative to the effective rate constant.

In figure 4.4, we show the emission rate calculated using (3.74) and the effective rate constants in figure 4.3a. Note that we have normalized the emission rate to the initial emission rate $I_0 = I(t = 0)$. The intensity of the beam is significantly reduced within the first second. This could have been anticipated, since the lifetime of the vibration assisted tunneling and the two highest energy levels are less than a millisecond. Hence, the resulting beam after a few seconds essentially consists of molecules in the ground state and the first excited state.

We also see in figure 4.4 that the emission rate is asymptotically approaching the emission rate of the ground state. However, the higher the initial temperature the longer it takes to reach the asymptotic behavior. This is as expected since higher initial temperature gives a broader internal temperature distribution, hence more particles with high internal temperature.

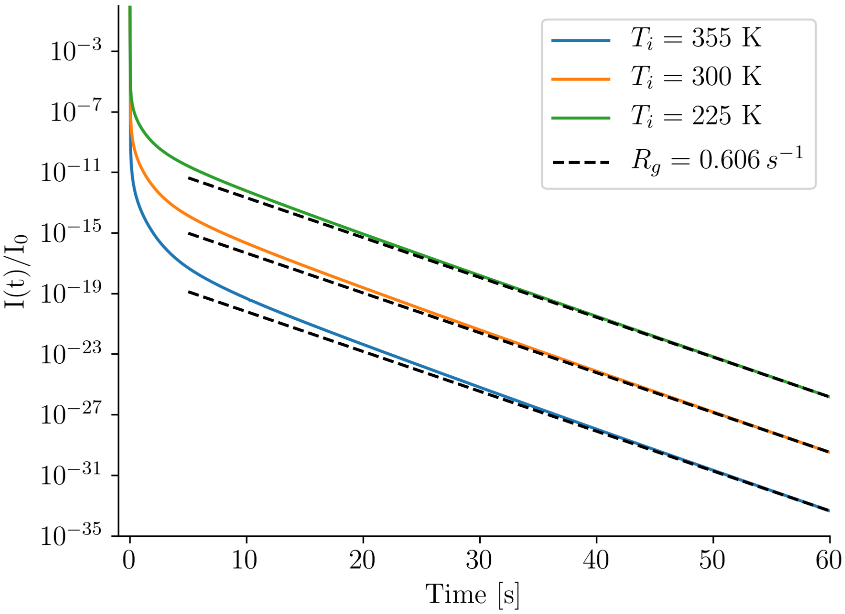

Figure 4.4: The intensity as a function of time for three initial temperatures. The dashed lines show the ground state decay rate normalized to visualize the asymptotic behavior.

4.3 Emission rate of C_{60}^{2-} for different ℓ values

To better understand how the emission rate depends on the angular quantum number, we focus on $\ell < 3$ for a fixed initial temperature $T_i = 300$ K. In table 4.2, we have tabulated the energy levels and the decay rates used in the Arrhenius decay for the vibrational assisted tunneling, as described in 4.2.

We calculate the emission rate for $T_i = 300$ K and $\ell < 3$. See figure 4.5. The behavior is similar to that in figure 4.4 where we have a rapid initial decay and the asymptotic behavior for $t \to \infty$, where the emission rate is approaching the emission rate of the ground state.

Table 4.2: The vibrational assisted tunneling levels for the different potentials and their individual decay rate.

	Energy [eV]	Decay rate [s^{-1}]
$\ell = 0$	0.450	6.08×10^7
1	0.452	2.73×10^7
2	0.456	5.84×10^6

The slope of the asymptot depends heavily on the ℓ value which is expected from the large variation of the decay rate for the ground state in table 4.1. We also see that the time it takes to reach the asymptotic behavior depends on the ℓ value, where larger ℓ results in a longer time before reaching the asymptotic behavior.

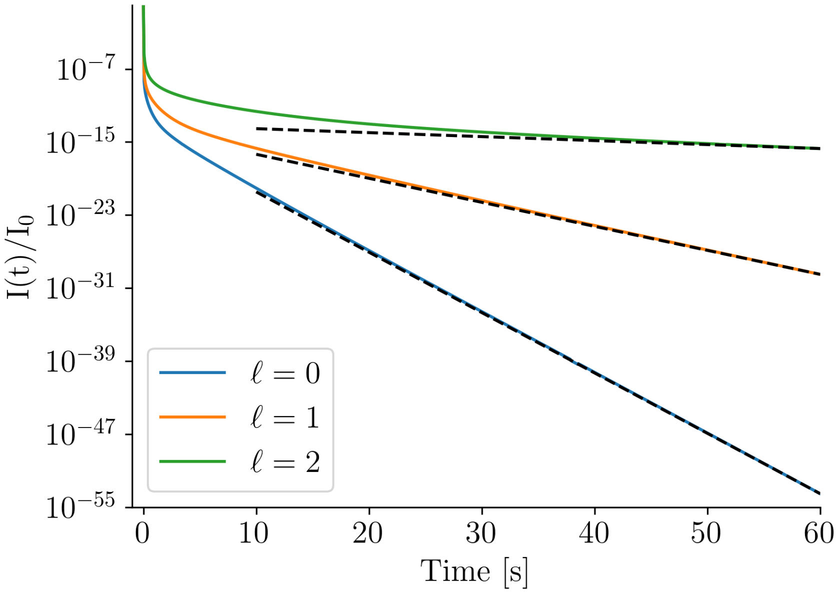

Figure 4.5: Emission rate as a function of time for $T_i = 300$ K and $\ell < 3$. The dashed lines show the ground state emission rates for each of the different potentials.

Chapter 5

Conclusion

In this thesis, we used a simple theoretic model to calculate the emission rate of C_{60}^{2-}. We found that the decay rate of the two highest excited states are four to five orders of magnitude larger than that of the ground state. This leads to a rapid decay within the first second and an asymptotic approach to the emission rate of the ground state as $t \to \infty$. The time it takes to reach the asymptotic behavior depends on the initial temperate, where higher initial temperature leads to longer times before reaching the asymptotic behavior.

We also found that the asymptotic behavior depends heavily on the angular quantum number ℓ, where larger ℓ value leads to smaller decay rate. The time it takes to reach the asymptotic behavior of the emission rate of the ground state also depends on the ℓ value, where larger ℓ value leads to longer times before reaching the asymptotic behavior. However, the asymptotic behavior is reached within a minute and it should therefore be possible to measure the decay rate of the ground state at the DESIREE facility.

In summary, we have mainly focused on the asymptotic behavior of the emission rate as it approaches the emission rate of the ground state. However, for future work it would be interesting to take a closer look at the initial behavior for times much less than a second. In this region it is thought that the emission rate has an approximate $\frac{1}{t}$ dependence [6].

Bibliography

[1] H. W. Kroto and R. W. David, "Fullerene," (Accessed: May 05, 2020), https://www.britannica.com/science/fullerene.

[2] S. Tomita, J. Andersen, H. Cederquist, B. Concina, and O. E. Echt, J. Chem. Phys **124** (2006).

[3] H. Zettergren, B. O. Forsberg, and H. Cedequist, Phys. Chem. Chem. Phys. **14**, 16360 (2012).

[4] B. Zwiebach, *Semiclassical approximation* (Massachusetts Institute of Technology: MIT OpenCourseWare, https://ocw.mit.edu/. License: Creative Commons BY-NC-SA, 2018).

[5] J. Andersen, C. Gottrup, K. Hansen, P. Hvelplund, and M. Larsson, Eur. Phys. J. D **17**, 189 (2001).

[6] J. U. Andersen, E. Bonderup, and K. Hansen, Journal of Physics B: Atomic, Molecular and Optical Physics **35** (2002).

[7] W. H. G. Jr., S. M. G. G. Fitzgerald, P. W. Fowler, A. Ceulemans, and B. C. Titeca, J. Phys. Chem. **100**, 14892 (1996).

[8] Q. Shi and S. Kais, Molecular Physics **100:4**, 475 (2002).